Geochemical Perspectives Letters

Co-reduction of Fe(III) and S^0 drives Fe-S biomineral formation and phosphate mobilisation

R. Bronner[1#], K. Thompson[2#], C. Dreher[1], E. Runge[3], E. Voggenreiter[1], J. Shuster[4], B. Wan[1], P. Joshi[1], S. Fischer[4], J.-P. Duda[3], A. Kappler[1,5], M. Mansor[1*]

https://doi.org/10.7185/geochemlet.2301

Abstract

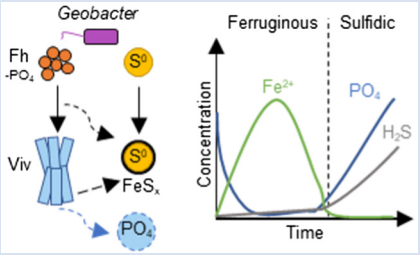

Microbially mediated iron and sulfur cycling have impacted redox transitions and the bioavailability of nutrients throughout Earth's history. Here, we incubated *Geobacter sulfurreducens* in the co-presence of ferrihydrite and S^0 at pH 6.5, 7.2 or 8.0. Microbial reduction of Fe(III) and S^0 resulted in a shift from ferruginous (Fe^{2+}-rich) to sulfidic (sulfide-rich) conditions and the precipitation of mackinawite, greigite and vivianite. The initial pH controlled the timing of the ferruginous-sulfidic transition and the relative abundance and crystallinity of the formed minerals. Vivianite formation was attributed to phosphate initially added to the medium. Phosphate showed a dynamic cycle, with low dissolved concentrations initially due to sorption to ferrihydrite, followed by vivianite precipitation under ferruginous conditions, and a significant release under sulfidic conditions. Co-reduction of Fe(III) and S^0 therefore regulates Fe-S biomineral formation and P bioavailability, which could be particularly important to consider in microbial mats and the sulfate-poor Archean ocean.

Received 15 September 2022 | Accepted 12 December 2022 | Published 17 January 2023

Introduction

Microbially mediated Fe and S cycling are vital parts of Earth's history that affected the oceanic transition between ferruginous and sulfidic conditions, as well as playing an integral role in modern biogeochemical cycles of greenhouse gases, nutrients and contaminants (Lepot, 2020; Kappler *et al.*, 2021). Many species, including model organisms *Geobacter* and *Shewanella*, are capable of linking the Fe and S cycles through the reduction of Fe(III) minerals and elemental sulfur (S^0). This metabolic flexibility enables them to survive under alkaline conditions when Fe(III) reduction becomes thermodynamically unfeasible (Flynn *et al.*, 2014), resulting in Fe sulfide biomineral formation (Wang *et al.*, 2018; Nie *et al.*, 2020; Ye and Jing, 2022; Liu *et al.*, 2023). Investigations of coupled reduction of Fe(III) and S^0 are important for mineral biosignatures and their impact on nutrient bioavailability, especially in environments where S^0 could be an important electron acceptor such as in microbial mats and sulfate-poor Archean oceans (Troelsen and Jørgensen, 1982; van Gemerden *et al.*, 1989; Philippot *et al.*, 2007; Galić *et al.*, 2017). The mobilisation and bioavailability of phosphate in particular is affected by Fe and S biogeochemistry with direct consequences to primary productivity, climate and Earth's redox evolution (Alcott *et al.*, 2022).

Microbial Metabolism Drives Geochemical Shifts

To investigate biomineral formation during co-reduction of Fe(III) and S^0, *G. sulfurreducens* was incubated in the co-presence of ferrihydrite (30 mM) and S^0 (60 mM) with acetate as excess electron donor. Different initial pH values (6.5, 7.2 or 8.0) were employed. Over 42 days of incubation, all cultures exhibited a colour change from dark brown to black, indicating transformation of ferrihydrite to reduced Fe minerals (Fig. S-1). From initial pH values of 6.5 and 7.2, pH increased to 7.1 and 7.5, respectively. At initial pH of 8.0, the pH slightly decreased to 7.9. From here onward, the cultures will be referred to by their initial pH values for simplicity.

At the beginning, solid phase extractable Fe (6 M HCl) amounted to 29.1 ± 2.2 mM ($n = 12$) with no Fe(II) components detected. Within 15 days, the Fe(II)/Fe(III) percentages of the HCl extractable Fe approached 100 %, indicating Fe(III) reduction (Fig. S-2). Note that the total HCl extractable Fe decreased over time, and we attributed this primarily to sampling inhomogeneity due to mineral aggregation. Fe(III) reduction was accompanied by the release of Fe^{2+} into solution, reaching maxima of 1000–2000 µM depending on initial pH (Fig. 1). Dissolved Fe^{2+} showed a decline to <500 µM within 12 days after the maximum. Once Fe^{2+} reached low levels, dissolved sulfide started to

1. Geomicrobiology, Center for Applied Geosciences, University of Tuebingen, 72076 Tuebingen, Germany
2. Microbial Ecology, Center for Applied Geosciences, University of Tuebingen, 72076 Tuebingen, Germany
3. Sedimentology and Organic Geochemistry, Center for Applied Geosciences, University of Tuebingen, 72076 Tuebingen, Germany
4. Tuebingen Structural Microscopy Core Facility, University of Tuebingen, 72076 Tuebingen, Germany
5. Cluster of Excellence: EXC 2124: Controlling Microbes to Fight Infection, Tuebingen, Germany
Co-first authors
* Corresponding author (email: muammar.muammar-bin-mansor@uni-tuebingen.de)

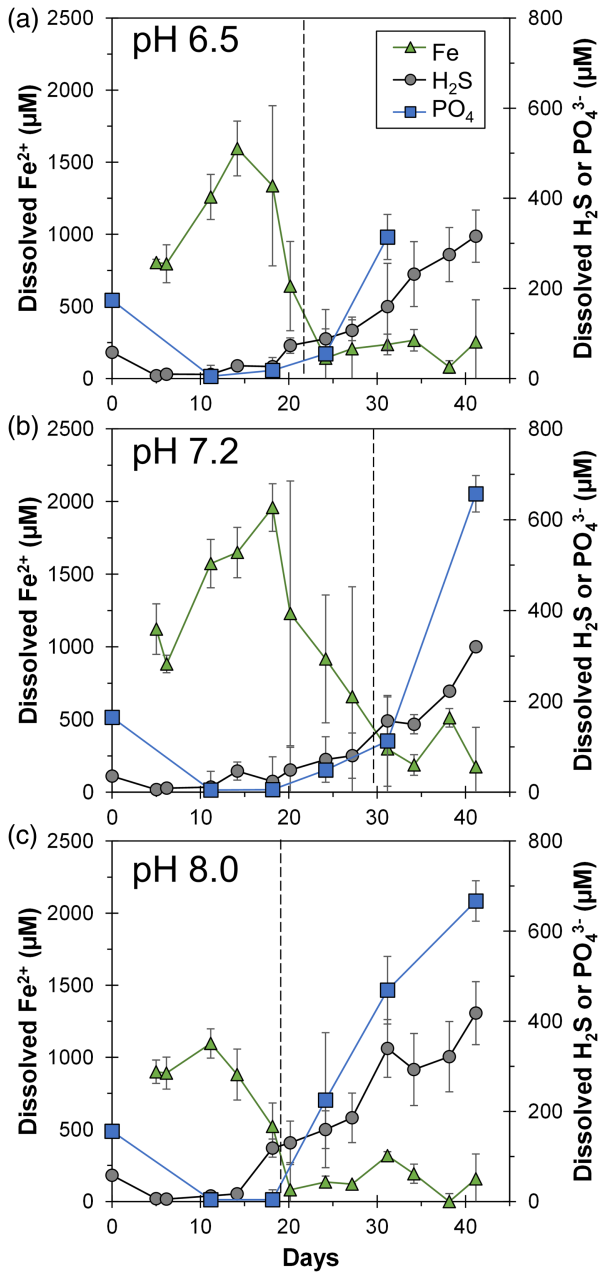

Figure 1 Geochemical evolution of dissolved Fe^{2+}, total sulfide and phosphate at **(a)** pH 6.5, **(b)** pH 7.2, and **(c)** pH 8.0. Dashed vertical lines denote the shift from ferruginous to sulfidic conditions.

increase, reaching maxima of 320–420 μM. Solid phase Fe sulfides were not quantified but were detectable by scanning electron microscopy (SEM), X-ray diffraction (XRD) and Mössbauer spectroscopy (Figs. 2, 3).

Overall, cultures at different pH values exhibited similar geochemical trends with differences in timing and the amount of Fe^{2+} and sulfide released to the solution. Parallel abiotic controls showed neither Fe(II) nor sulfide production (Fig. S-2). The geochemical evolution can be divided into two stages. In the first stage, *ferruginous conditions* dominated as ferrihydrite was reduced and Fe^{2+} accumulated in solution. In the second stage, *sulfidic conditions* were observed once reactive Fe(III) surfaces were exhausted and sulfide accumulated in solution. The time at which the shift from ferruginous to sulfidic conditions occurred differed depending on the pH values, following the order: pH 7.2 (30 days) > pH 6.5 (22 days) > pH 8.0 (19 days). Mirroring this trend, the highest maximum Fe^{2+} followed the order: pH 7.2 (2000 μM) > pH 6.5 (1500 μM) > pH 8.0 (1100 μM). Maximum dissolved sulfide followed the opposite trend: pH 7.2 ≈ pH 6.5 (320 μM) < pH 8.0 (420 μM).

The different timings and concentrations of Fe^{2+} and sulfide observed depend on a number of interrelated pH dependent processes including microbial preference of Fe(III) over S^0, Fe^{2+} adsorption to ferrihydrite, sulfide mediated ferrihydrite reduction and Fe mineral precipitation. These processes can lead to secondary phenomena such as Fe^{2+} catalysed recrystallisation, decreased reactivity from the FeS surface coating, and formation of polysulfides (Peiffer *et al.*, 2015). Notably, the observed geochemical trends do not follow straightforward predictions based on initial pH (Supplementary Information). Further extensive investigation at the nanometre (*e.g.*, transmission electron microscopy) and molecular (*e.g.*, speciation *via* synchrotron) scales, coupled to a biogeochemical model will be needed to elucidate the specific mechanisms.

Formation of Biogenic Mackinawite and Greigite, but not Pyrite

Mineral products were identified using a combination of magnetic testing, XRD, SEM and Mössbauer spectroscopy. XRD patterns of samples at day 21 and 42 indicated the presence of S^0, which decreased over time at all pH values, signifying continuous microbial S^0 reduction (Fig. 3a). Additionally, XRD and Mössbauer identified mackinawite (FeS) as a major product (20–70 % of solid phase Fe). Black colourations typical of Fe sulfides were commonly observed to form coatings on S^0 (Fig. 2c, d).

We report the first instance of greigite (Fe_3S_4) formation by *Geobacter*. The presence of a magnetic mineral was first suggested *via* attraction of the minerals to a hand magnet held next to the bottles. Strong magnetism was observed at all pH values starting from day 11 (Fig. S-1) but decreased noticeably after 27 days (Supplementary Information). Greigite was identified by Mössbauer spectroscopy, making up 17–53 % of solid phase Fe with the highest percentage at pH 7.2. XRD data showed clear patterns for greigite only at pH 6.5 at day 21. Positive identification in other cultures was complicated due to the overlap of the main greigite signal with mackinawite at ~35° 2θ and the generally broad patterns resulting from low crystallinity. Consistent with this interpretation, crystalline greigite particles were not observed by SEM. Other minerals such as magnetite (Fe_3O_4) and pyrite were not detectable within 21–42 days of incubation (Supplementary Information).

The mechanism and kinetics of biogenic Fe sulfide mineral transformation are important to understand with respect to their implications for biosignatures and elemental cycling (Picard *et al.*, 2016; Nie *et al.*, 2020). Poorly-crystalline mackinawite typically forms first from the reaction between Fe^{2+} and sulfide at low temperatures, followed by its transformation to greigite and pyrite over time (Son *et al.*, 2022). In our cultures, the XRD patterns for mackinawite were most pronounced at pH 7.2, and inspection of the main signal at ~18° 2θ showed that it became broader over time at all pH values, suggesting an overall decrease in bulk crystallinity. This can be understood in terms of different populations of mackinawite that formed under ferruginous *versus* sulfidic conditions. Mackinawite formed in excess Fe (ferruginous conditions) tends to exhibit higher crystallinity and sharper diffraction patterns than that formed in excess S (sulfidic conditions) (Bourdoiseau *et al.*, 2008). This is consistent with the timing of the stages in our cultures. The pH 7.2 cultures had the longest ferruginous stage that encompassed the period at which the first XRD samples were collected (21 days); therefore,

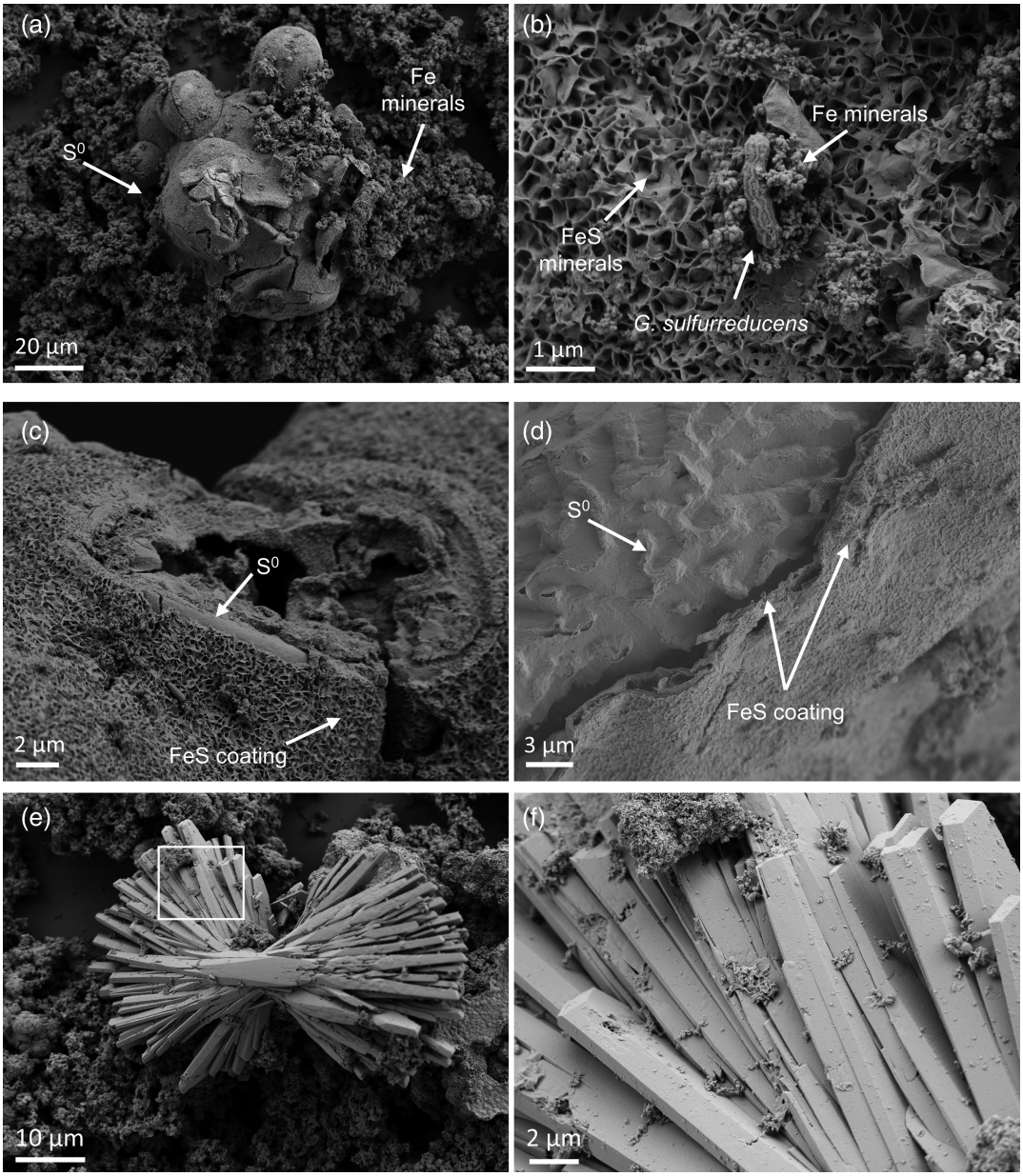

Figure 2 SEM micrographs of microbe-mineral associations. **(a)** S^0 aggregates consisting of ~20 µm globules and Fe mineral aggregates consisting of nanometre-sized structures. **(b)** *G. sulfurreducens* atop a S^0 globule. Note the close spatial association with aggregates of Fe-O minerals and FeS-rich minerals with pseudo-honeycomb structure. **(c)** A naturally fractured sample highlighting the FeS-rich coating on a S^0 globule. **(d)** The FeS-rich coating appeared to peel off, revealing the smoother surface texture of S^0 compared to FeS. **(e)** Typical morphology of Fe-P-O-rich minerals (vivianite). **(f)** A higher magnification of the radial blade-like morphology of vivianite (from the boxed region in **(e)**).

crystalline mackinawite is expected. With longer incubation, the cultures shifted to sulfidic conditions, promoting additional mackinawite formation. However, this mackinawite exhibited lower crystallinity and contributed to broader XRD patterns reflective of the bulk mixture.

Greigite is increasingly recognised as a common and stable phase in nature and as an important intermediate for pyrite formation (Subramani *et al.*, 2020). We found the highest percentage of greigite at the intermediate pH of 7.2 (53 % of solid phase Fe). This is in contrast with the expectation that lower pH, including around the microenvironments of sulfate reducing bacteria, could promote mackinawite's transformation to greigite (Bourdoiseau *et al.*, 2011; Mansor *et al.*, 2019). Instead of pH, we suggest that the crystallinity of the precursor mackinawite is the main controlling factor of transformation kinetics (Csákberényi-Malasics *et al.*, 2012; Miller *et al.*, 2020). As discussed, we observed mackinawite with the highest crystallinity at pH 7.2. Our data showed that precipitation under ferruginous conditions enhances mackinawite's crystallinity and its transformation to greigite, confirming recent predictions from density functional theory (Son *et al.*, 2022).

Pyrite, the most common Fe sulfide mineral in the environment, was not formed in our cultures within 42 days, similar to in pure cultures of sulfate reducing bacteria (Picard *et al.*, 2016). Nonetheless, studies with sulfur cycling bacteria have demonstrated pyrite formation from sulfidation of Fe(III) phosphates within one month (Berg *et al.*, 2020; Duverger *et al.*, 2020). Pyrite precipitation was attributed to microbial production of

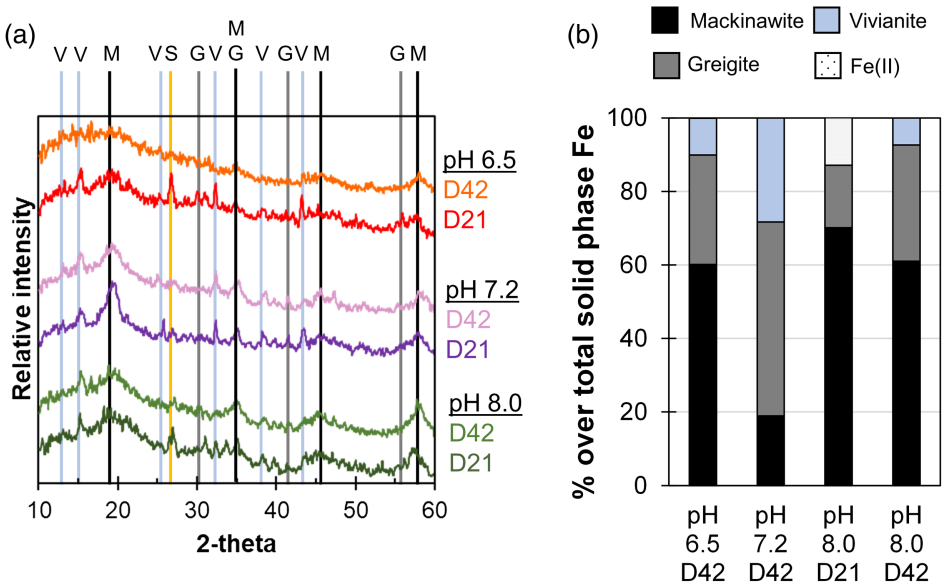

Figure 3 **(a)** XRD patterns of precipitates at Days (D) 21 and 42. Vertical lines denote 2θ positions specific to certain minerals, with colours corresponding to vivianite ('V', light blue), mackinawite ('M', black), S^0 ('S', yellow) and greigite ('G', grey). **(b)** Solid phase Fe distribution based on Mössbauer spectroscopy at 77 K.

extracellular polymeric substances (EPS) that concentrated key ingredients for pyrite formation locally and the continuous formation of Fe^{2+}, S^0 and polysulfides from slow sulfide mediated Fe(III) dissolution. *G. sulfurreducens* is also known to produce EPS that can bind cations, especially in the presence of Fe(III) minerals (Stöckl *et al.*, 2019; Tomaszewski *et al.*, 2020). Furthermore, the co-presence of Fe(III) and S^0 should have led to high polysulfide concentrations that enhance pyrite formation. However, it is possible that rapid reduction of Fe(III) and S^0 (and potentially polysulfides) by *G. sulfurreducens* may have prevented the accumulation of intermediates necessary for fast pyrite formation. Further kinetic based studies and comparison with a pyrite forming culture will be necessary to elucidate factors controlling pyrite formation (Supplementary Information).

Microbial Fe-S Metabolism leads to Phosphate (Im)Mobilisation

Besides Fe sulfides, XRD and Mössbauer spectroscopy revealed the presence of vivianite [$Fe_3(PO_4)_2 \cdot 8\ H_2O$] at all pH values, making up 7–28 % of solid phase Fe (Fig. 3). The formed vivianite had radial blade-like structures up to 50 µm in length (Fig. 2e, f). Vivianite formation is explained by the addition of phosphate to the medium, which resulted in P/Fe ratio of 0.15 in our experiments, comparable to the ~0.10 ratio typical in nature (Kraal *et al.*, 2022).

Despite the addition of 4.4 mM phosphate, initial dissolved phosphate was <200 µM (Fig. 1). We attributed this to strong phosphate adsorption to ferrihydrite (Wang *et al.*, 2013; Kraal *et al.*, 2022). The concentrations dropped within a few days to near detection limit, coincident with the rise in Fe^{2+}, attributed to vivianite formation. Dissolved phosphate then showed a marked increase coincident with sulfide release to solution.

The sequence of biogeochemical processes in the experiments can be summarised as follows (Fig. 4). First, phosphate from the growth medium was rapidly adsorbed to ferrihydrite. *G. sulfurreducens* reduced ferrihydrite and S^0 in the presence of excess electron donor, with more S^0 reduction at pH 8.0 compared to lower pH values. In the early ferruginous stage, sulfide concentration was kept low as it reacted rapidly with ferrihydrite, contributing to Fe(III) reduction, Fe^{2+} release to solution, and the precipitation of mackinawite, greigite and vivianite. The cultures progressed into the late sulfidic stage as reactive Fe(III) became fully exhausted. In addition to further Fe sulfide formation, this biogeochemical switch resulted in vivianite dissolution, releasing phosphate into solution. This supports previous observations in which the switch from ferruginous to sulfidic conditions has been recognised to increase the bioavailability of phosphate (Duverger *et al.*, 2020; Alcott *et al.*, 2022).

Overall, our study demonstrated that co-reduction of Fe(III) and S^0 leads to formation of mackinawite, greigite and vivianite, but not pyrite within 42 days. Initial pH affected the length and timing of the ferruginous-sulfide transition, resulting in differences in the crystallinity and relative abundance of the mineral products. The transition from ferruginous to sulfidic

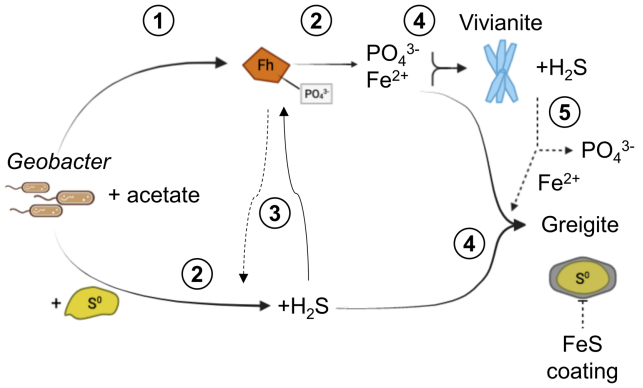

Figure 4 Summary of biogeochemical processes in the cultures. (1) Adsorption of phosphate from growth medium onto ferrihydrite (Fh). (2) Concurrent reduction of Fh and S^0 by *G. sulfurreducens*. (3) Sulfide mediated reduction of Fh. (4) Precipitation of vivianite, mackinawite and greigite. (5) Dissolution of vivianite by H_2S, releasing phosphate into solution.

conditions was associated with phosphate release. Similar processes, driven by the activity of whole microbial communities instead of a single species, are likely important to consider for micro-niches in modern sediments and microbial mats. These processes are further applicable to SO_4-poor Archean oceans and ultimately the investigation of Fe-S biomineral signatures and the bioavailability of important nutrients that affected primary productivity and Earth's biogeochemical evolution.

Acknowledgements

This study was supported by the DFG (SPP 1833, Emmy Noether Programme, 1450/3-1, DU 1450/3-2, DU 1450/7-1, JPD; INST 37/1027-1 FUGG, AK) as well as the Excellence Strategy of the German Federal and State Governments (EXC2124, 390838134; Tuebingen Structural Microscopy Core Facility; AK, MM, PJ, SF, JS). We thank Prof. D.J. Lunter and Yali Liu for assistance with Raman analysis.

Editor: Juan Liu

Additional Information

Supplementary Information accompanies this letter at https://www.geochemicalperspectivesletters.org/article2301.

Cite this letter as: Bronner, R., Thompson, K., Dreher, C., Runge, E., Voggenreiter, E., Shuster, J., Wan, B., Joshi, P., Fischer, S., Duda, J.-P., Kappler, A., Mansor, M. (2023) Co-reduction of Fe(III) and S^0 drives Fe-S biomineral formation and phosphate mobilisation. *Geochem. Persp. Let.* 24, 27–32. https://doi.org/10.7185/geochemlet.2301

References

Alcott, L.J., Mills, B.J.W., Bekker, A., Poulton, S.W. (2022) Earth's Great Oxidation Event facilitated by the rise of sedimentary phosphorus recycling. *Nature Geoscience* 15, 210–215. https://doi.org/10.1038/s41561-022-00906-5

Berg, J.S., Duverger, A., Cordier, L., Laberty-Robert, C., Guyot, F., Miot, J. (2020) Rapid pyritization in the presence of a sulfur/sulfate-reducing bacterial consortium. *Scientific Reports* 10, 8264. https://doi.org/10.1038/s41598-020-64990-6

Bourdoiseau, J.-A., Jeannin, M., Sabot, R., Rémazeilles, C., Refait, P. (2008) Characterisation of mackinawite by Raman spectroscopy: Effects of crystallisation, drying and oxidation. *Corrosion Science* 50, 3247–3255. https://doi.org/10.1016/j.corsci.2008.08.041

Bourdoiseau, J.-A., Jeannin, M., Rémazeilles, C., Sabot, R., Refait, P. (2011) The transformation of mackinawite into greigite studied by Raman spectroscopy. *Journal of Raman Spectroscopy* 42, 496–504. https://doi.org/10.1002/jrs.2729

Csákberényi-Malasics, D., Rodriguez-Blanco, J.D., Kis, V.K., Rečnik, A., Benning, L.G., Pósfai, M. (2012) Structural properties and transformations of precipitated FeS. *Chemical Geology* 294–295, 249–258. https://doi.org/10.1016/j.chemgeo.2011.12.009

Duverger, A., Berg, J.S., Busigny, V., Guyot, F., Bernard, S., Miot, J. (2020) Mechanisms of Pyrite Formation Promoted by Sulfate-Reducing Bacteria in Pure Culture. *Frontiers in Earth Science* 8, 588310. https://doi.org/10.3389/feart.2020.588310

Flynn, T.M., O'Loughlin, E.J., Mishra, B., DiChristina, T.J., Kemner, K.M. (2014) Sulfur-mediated electron shuttling during bacterial iron reduction. *Science* 344, 1039–1042. https://doi.org/10.1126/science.1252066

Galić, A., Mason, P.R.D., Mogollón, J.M., Wolthers, M., Vroon, P.Z., Whitehouse, M.J. (2017) Pyrite in a sulfate-poor Paleoarchean basin was derived predominantly from elemental sulfur: Evidence from 3.2 Ga sediments in the Barberton Greenstone Belt, Kaapvaal Craton. *Chemical Geology* 449, 135–146. https://doi.org/10.1016/j.chemgeo.2016.12.006

Kappler, A., Bryce, C., Mansor, M., Lueder, U., Byrne, J.M., Swanner, E.D. (2021) An evolving view on biogeochemical cycling of iron. *Nature Reviews Microbiology* 19, 360–374. https://doi.org/10.1038/s41579-020-00502-7

Kraal, P., van Genuchten, C.M., Behrends, T. (2022) Phosphate coprecipitation affects reactivity of iron (oxyhydr)oxides towards dissolved iron and sulfide. *Geochimica et Cosmochimica Acta* 321, 311–328. https://doi.org/10.1016/j.gca.2021.12.032

Lepot, K. (2020) Signatures of early microbial life from the Archean (4 to 2.5 Ga) eon. *Earth-Science Reviews* 209, 103296. https://doi.org/10.1016/j.earscirev.2020.103296

Liu, Y., Zhao, Q., Liao, C., Tian, L., Yan, X., Li, N., Wang, X. (2023) Anaerobic bioreduction of elemental sulfur improves bioavailability of Fe(III) oxides for bioremediation. *Science of the Total Environment* 858, 159794. https://doi.org/10.1016/j.scitotenv.2022.159794

Mansor, M., Berti, D., Hochella Jr., M.F., Murayama, M., Xu, J. (2019) Phase, morphology, elemental composition and formation mechanisms of biogenic and abiogenic Fe-Cu-sulfide nanoparticles: A comparative study on their occurrences under anoxic conditions. *American Mineralogist* 104, 703–717. https://doi.org/10.2138/am-2019-6848

Miller, N., Dougherty, M., Du, R., Sauers, T., Yan, C., *et al.* (2020) Adsorption of Tetrathiomolybdate to Iron Sulfides and Its Impact on Iron Sulfide Transformations. *ACS Earth and Space Chemistry* 4, 2246–2260. https://doi.org/10.1021/acsearthspacechem.0c00176

Nie, Z., Wang, N., Xia, X., Xia, J., Liu, H., Zhou, Y., Deng, Y., Xue, Z. (2020) Biogenic FeS promotes dechlorination and thus de-cytotoxity of trichloroethylene. *Bioprocess and Biosystems Engineering* 43, 1791–1800. https://doi.org/10.1007/s00449-020-02369-7

Peiffer, S., Behrends, T., Hellige, K., Larese-Casanova, P., Wan, M., Pollok, K. (2015) Pyrite formation and mineral transformation pathways upon sulfidation of ferric hydroxides depend on mineral type and sulfide concentration. *Chemical Geology* 400, 44–55. https://doi.org/10.1016/j.chemgeo.2015.01.023

Philippot, P., Van Zuilen, M., Lepot, K., Thomazo, C., Farquhar, J., Van Kranendonk, M.J. (2007) Early Archaean Microorganisms Preferred Elemental Sulfur, Not Sulfate. *Science* 317, 1534–1537. https://doi.org/10.1126/science.1145861

Picard, A., Gartman, A., Girguis, P.R. (2016) What Do We Really Know about the Role of Microorganisms in Iron Sulfide Mineral Formation? *Frontiers in Earth Science* 4, 68. https://doi.org/10.3389/feart.2016.00068

Son, S., Hyun, S.P., Charlet, L., Kwon, K.D. (2022) Thermodynamic stability reversal of iron sulfides at the nanoscale: Insights into the iron sulfide formation in low-temperature aqueous solution. *Geochimica et Cosmochimica Acta* 338, 220–228. https://doi.org/10.1016/j.gca.2022.10.021

Stöckl, M., Teubner, N.C., Holtmann, D., Mangold, K.-M., Sand, W. (2019) Extracellular Polymeric Substances from *Geobacter sulfurreducens* Biofilms in Microbial Fuel Cells. *ACS Applied Materials and Interfaces* 11, 8961–8968. https://doi.org/10.1021/acsami.8b14340

Subramani, T., Lilova, K., Abramchuk, M., Leinenweber, K.D., Navrotsky, A. (2020) Greigite (Fe_3S_4) is thermodynamically stable : Implications for its terrestrial and planetary occurrence. *Proceedings of the National Academy of Sciences* 117, 28645–28648. https://doi.org/10.1073/pnas.2017312117

Tomaszewski, E.J., Olson, L., Obst, M., Byrne, J.M., Kappler, A., Muehe, E.M. (2020) Complexation by cysteine and iron mineral adsorption limit cadmium mobility during metabolic activity of *Geobacter sulfurreducens*. *Environmental Science: Processes and Impacts* 22, 1877–1887. https://doi.org/10.1039/D0EM00244E

Troelsen, H., Jørgensen, B.B. (1982) Seasonal dynamics of elemental sulfur in two coastal sediments. *Estuarine, Coastal and Shelf Science* 15, 255–266. https://doi.org/10.1016/0272-7714(82)90062-2

van Gemerden, H., Tughan, C.S., de Wit, R., Herbert, R.A. (1989) Laminated microbial ecosystems on sheltered beaches in Scapa Flow, Orkney Islands. *FEMS Microbiology Ecology* 5, 87–101. https://doi.org/10.1111/j.1574-6968.1989.tb03661.x

Wang, X., Liu, F., Tan, W., Li, W., Feng, X., Sparks, D.L. (2013) Characteristics of Phosphate Adsorption-Desorption Onto Ferrihydrite: Comparison With

Well-Crystalline Fe (Hydr)Oxides. *Soil Science* 178, 1–11. https://doi.org/10.1097/SS.0b013e31828683f8

Wang, X.-N., Sun, G.-X., Li, X.-M., Clarke, T.A., Zhu, Y.-G. (2018) Electron shuttle-mediated microbial Fe(III) reduction under alkaline conditions. *Journal of Soils and Sediments* 18, 159–168. https://doi.org/10.1007/s11368-017-1736-y

Ye, L., Jing, C. (2022) Iron(III) reducing bacteria immobilise antimonite by respiring elemental sulfur. *Geochemical Perspectives Letters* 21, 37–41. https://doi.org/10.7185/geochemlet.2215